Applied Surface Science 610 (2023) 155578

Contents lists available at ScienceDirect

Applied Surface Science

journal homepage: www.elsevier.com/locate/apsusc

Full length article

Advanced transmission electron microscopy investigation of defect formation in movpe-growth of gap on silicon using arsenic initial coverage

Amalia Navarro [a], Elisa García-Tabarés [a], Quentin M. Ramasse [b,c], Pablo Caño [d], Ignacio Rey-Stolle [d], Beatriz Galiana [a,*]

[a] Universidad Carlos III de Madrid, Departamento de Física, Avda. Universidad 30, 28911 Leganés, Madrid, Spain
[b] School of Chemical and Process Engineering, University of Leeds, Leeds LS2 9JT, UK
[c] SuperSTEM, Daresbury Laboratory, Keckwick Lane, Daresbury WA4 4AD, UK
[d] Instituto de Energía Solar, IES-UPM, ETSI. Telecomunicación, 28040 Madrid, Spain

ARTICLE INFO

Keywords:
III-V
Silicon
GaP
Stacking faults
Interface
MOVPE
AsH_3
HRTEM
STEM
EELS

ABSTRACT

Integration of GaP layers on silicon substrates using AsH_3 pre-exposure followed by a PH_3-based GaP epitaxial growth allows the development of very promising processes for the photovoltaic industry, although many of the growth routines using this approach suffer from reproducibility issues when transferred to a new epitaxial system, leading to poor quality layers. This fact reveals a lack of knowledge on the mechanisms behind the formation of the most common planar defects (stacking faults and microtwins) and their dynamics for GaP/Si Metal Organic Vapor Phase Epitaxy using AsH_3 and PH_3. Therefore, in this work, a set of GaP/Si samples with a similarly high defect density grown between 700 °C and 725 °C, are analyzed by means of high-resolution scanning transmission electron microscopy and electron energy loss spectroscopy. The results presented show contaminant-free Si surfaces for temperatures above 725 °C, ruling out the hypothesis of contaminant as the origin of these planar defects. Regarding the interface Si/GaP, the GaP growth starts, in all the samples, with Ga—Si bonds. Additionally, no traces of As are found, which reinforces the hypothesis of an effectively displacement of As on Si surface by Ga atoms at high temperature. Finally, it is observed complex chemical structures in the origin of the microtwins and the cause of the origin of these defects seems to be a localized gallium depletion at the GaP/Si interface.

1. Introduction

The integration of III-V semiconductors on silicon has been a long-sought goal for the microelectronic industry [1],[2] In the photovoltaic field, particularly, the integration of III-V compounds on Si was intensively investigated in the 1980s and 1990s. The work carried out in these decades pointed out that the main challenges for III-V heteroepitaxy on Si were: 1) lattice mismatch, 2) thermal mismatch, and 3) the ability to grow a polar III/V semiconductor on a non-polar substrate such as Si. In spite of notable results achieved during these years [3–6], the intensity of this research declined considerably in the late 90s due to the difficulties in improving material quality and the rapid progress of multijunction solar cell (MJSC) technology based on germanium.

However, there has recently been a renewed interest in the integration of III-V materials on Si, driven by the potential applications for photovoltaics. Currently, the most developed techniques for such integration are direct epitaxial growth [7–9], wafer bonding [10],[11] and mechanical stacking [12]. However, even though wafer bonding and mechanical stacking have given higher solar cell than direct epitaxial growth [13], this last one implies a significant cost reduction since no III-V substrates are required. Conversely, the direct epitaxial growth of III-V on Si presents some fundamental challenges among which are the appearance of defects such as antiphase domains (APDs), stacking faults (SFs) and microtwins (MTs).

In order to get a defect-free III-V layer on Si, there are different approaches. For example, V-grooves [14] or nanopatterned Si substrates [15] are used to achieve good quality GaAs layers grown directly on Si. Other strategy is to develop compositional graded buffers based on SiGe [16] or based on III-V materials, allowing to change gradually the lattice constant from Si to the desired III-V material [17].

A common approach for the latter route is the formation of a virtual III-V substrate by growing a GaP nucleation layer on the Si substrate.

* Corresponding author.
E-mail address: bgaliana@fis.uc3m.es (B. Galiana).

https://doi.org/10.1016/j.apsusc.2022.155578
Received 19 January 2022; Received in revised form 27 October 2022; Accepted 1 November 2022
Available online 8 November 2022

This heteroepitaxial growth (GaP/Si) has the minimum lattice mismatch for a III-V binary compound on Si, i.e. 0.37% at 300 K [18]. Eventually, this virtual substrate will act as a template for the growth of the complete III-V semiconductor structure. Despite the low lattice mismatch between both materials, it is well known that the GaP/Si system presents certain challenges that degrade the quality of the layers, namely: i) the epitaxial strain or three dimensional growth, that leads to the formation of defects at the GaP/Si heterointerface or/and in the epitaxial layer [19–21]; ii) the fact that the growth of a polar III-V semiconductor (i.e. GaP) on a non-polar substrate (i.e. Si) induces the formation of antiphase domains (APDs) [19],[20],[22],[23], which, if not avoided at the initial growth stage or annihilated through subsequent processing steps, will be detrimental for device performance; and iii) the unwanted cross-doping through the III-V/Si heterointerface [6],[24].

In this respect, it can be stated that there are three main requirements that need to be fulfilled to achieve a successful growth of GaP on Si: i) the formation of a pristine Si surface prior to growth, free of any trace contaminants, especially C and O, since they can behave as nucleation centers for defects at the GaP/Si interface; ii) to avoid the formation of APDs to minimize the creation of other structural defects (such as SFs and MTs that could reach the surface and degrade the device), by using Si (111) substrates [25], V-grooves Si [26] or misoriented Si (001) to promote the formation of a single-domain double-stepped Si surface [18],[24],[27],[28], and finally iii) a good control of GaP morphology to prevent defects from reaching the surface by promoting 2D growth or other strategies based on selective area growth using nanopatterned substrates [29].

To achieve a contaminant-free Si surface together with the formation of a double-stepped Si surface, there are mainly three well-reported strategies: i) a chemical cleaning and a subsequent thermal treatment at high temperature under hydrogen in metalorganic vapor-phase epitaxy (MOVPE) (about 950 °C) or under vacuum in molecular beam epitaxy (about 800 °C) [30], ii) the growth of a homoepitaxial Si buffer and subsequent annealing under hydrogen in MOVPE or under vacuum in MBE [18],[24],[31], and iii) a pre-exposure to either group III or V elements with the aim of growing a monolayer (ML) of Ga, As or P, which is the approach that we will address in this work.

Regarding the pre-nucleation step there is a wide range of empirical approximations [32] since a perfectly clean, oxide-free, single domain Si surface with double steps might not be enough to guarantee defect-free 2D GaP growth. When films are grown by MOVPE, most methodologies are based on group-V exposure since the adsorption of group V elements with high vapor pressure on the surface is a self-limited phenomenon, contrarily to exposure to group III atoms that tend to form clusters. However, it should be noted that the intensity of such group-V exposure should be carefully dosed since both AsH_3 or PH_3 can etch (i.e. roughen) the surface. The use of a phosphorus ML, either at high temperature [3],[33],[34] or low temperature [22],[35] has been the most commonly reported strategy. However, there have also been reports of the beneficial effects of exposing Si samples to an AsH_3 flush, under certain conditions, prior to the epitaxial growth of the GaP layer [27],[28],[36–38]. Hereinafter, we will refer to such AsH_3 flush as *AsH_3 pre-exposure*, as it takes place before the growth. The advantages of AsH_3 vs. PH_3 as a cleaning and surface conditioning agent prior to the GaP growth are: (i) AsH_3 provides a higher concentration of atomic hydrogen due to the lower pyrolysis temperature (i.e. higher cracking rate), as compared to PH_3. This H removes C and O from the surface, presumably by forming volatile species such as CH_4 and H_2O [36],[39] and (ii) As dimers released from AsH_3 pyrolysis form self-limiting, flat, (2 × 1) or (1 × 2) reconstructed surfaces on the Si wafer without the creation of stable Si—As compounds (contrarily to the Si—P compounds) [38], and thus better preserve the surface morphology against H-induced roughening (i.e. etching) [39]. Nevertheless, as noted above, a successful hydride pre-exposure –either with AsH_3 or PH_3– requires the precise determination of the optimum specific dosage to get the desired surface reconstruction while avoiding etching. In both cases, the excess or lack of exposure will negatively affect the silicon surface and, therefore, inevitably, the quality of the GaP subsequently grown [27],[36],[39] although, this process seems, in general, more controllable with AsH_3.

Although defect-free 2D growth using this approach has been reported [27], it is also known that similar conditions in analogous MOVPE reactors lead to GaP layers with poor morphological and structural quality. This suggests that either small reactor differences, growth history (also termed a 'memory effect') and/or subtle differences in the preparation or even quality of the substrate play a role in achieving a successful epitaxial growth recipe. Consequently, the achievement of a reproducible process in different environments is still an open issue in the development of GaP on Si using AsH_3 pre-exposure, mostly due to the uncertainties in the relation between growth conditions and nucleation mechanisms.

To address this issue, some authors have recently published results to clarify the phenomenon behind defect formation dynamics in GaP on Si low temperature MOVPE growth (around 500 °C) using TBP as group-V precursor for the pre-exposure and the GaP growth [40–42]. Conversely, there is a lack of equivalent studies for high temperature MOVPE growth using hydrides as group-V precursors (AsH_3 and PH_3) for the pre-exposure and the GaP growth.

Consequently, this paper does not aim to propose an optimal MOVPE routine to get a high-quality GaP nucleation layer on silicon, but rather to provide understanding in what triggers the formation of structural defects, frequently observed on this type of III-V structures that limit the reproducibility and applicability of the optimized routines, which could eventually be transferred to the photovoltaic industry under these growth conditions (temperature above 700 °C, AsH_3 pre-exposure and GaP growth using PH_3).

For that purpose, a set of samples presenting similar poor morphologies (i.e. 3D growth and high density of defects), but grown under different conditions, were characterized by means of transmission electron microscopy (TEM), high-resolution transmission electron microscopy (HRTEM), high resolution scanning transmission electron microscopy (STEM) and electron energy loss spectroscopy (EELS). In particular, AsH_3 pre-exposure parameters (i.e. temperature, and time) were varied.

2. Materials and methods

Epilayers of GaP were prepared using a horizontal AIX200/4 MOVPE reactor on mis-oriented Si (100) substrates. Wafers were deoxidized using an HF-dip for 3 min and preheated at 775 °C in a H_2 flow for 30 min to remove any residual traces of silicon oxide and to promote surface reconstruction. Before the initiation of the GaP growth, the substrates were subjected to an AsH_3 pre-exposure of 50 sccm at temperatures in the range of 700–725 °C. GaP layers were grown using PH_3 and TMGa as precursors during 330 s with a V/III ratio of 2000 and a growth rate of ~ 1 μm/h, using in each case the same temperature as for the AsH_3 pre-exposure. Reactor pressure was kept at 100 mbar for all the samples. These growth conditions were discussed in detail and optimized elsewhere [37]. In summary, the pre-exposure AsH_3 conditions used (time and temperature) are derived from an optimization process based on the analysis of in situ measurements using Reflectance Anisotropy Spectroscopy (RAS). This analysis determined that at 700–725 °C the resulting surface presented the expected RAS features for a Si wafer uniformly covered with consistently oriented As dimers, forming a single domain (i.e. a RAS signal with two strong peaks with energies at 2.9–3.4 eV and 3.6–3.9 eV [27],[43], and intensities ΔR/R between 1 and 2). Table I lists the AsH_3 pre-exposure parameters for each sample.

The characterization of the GaP crystals was carried out using TEM and STEM. Samples were prepared in cross-section by standard sample preparation methods, mechanical thinning and argon ion milling to electron transparency. The morphology and type of defects of the GaP crystals were examined in a Tecnai F20 operated at 200 kV. The

Table I
Description of the MOVPE AsH_3 pre-exposure routine.

Sample	AsH_3 pre-exposure		Miscut towards (111) plane
	Time (s)	Temperature (°C)	
1	150	700	6° [110]
2	150	725	2° [110]

microstructure of the GaP crystals was determined by means of HRTEM images and the corresponding spot patterns obtained by Fast Fourier Transform (FFT). The chemical composition at the GaP/Si interfaces was studied using high angle annular dark field (HAADF) imaging together with electron energy loss spectroscopy (EELS) in a Nion UltraSTEM100 aberration-corrected microscope operated at 100 kV. For the latter, the optics were configured for an electron probe of 31 mrad convergence semi-angle and 50 pA of beam current; the angular range of the HAADF detector was 90–185 mrad, while the EELS collection aperture semi-angle was 36 mrad. To provide high signal-to-noise data, and unless otherwise stated, micrographs presented below were generated by acquiring series of HAADF images consecutively prior to averaging using rigid registration techniques. EELS data was denoised using principal component analysis (as implemented in Gatan's Digital Micrograph software suite). Maps were obtained by integrating over the relevant ionization edges at suitable energy ranges, after removing the decaying background using a conventional power-law model.

3. Results & discussion

As previously described, the purpose of this study is to determine the main mechanisms that control the formation of common 3D crystal defects that appear when GaP is grown on Si at high temperature using AsH_3 pre-exposure. Discovering the causes that underlie the formation of defects is a key aspect to eventually prevent their occurrence. For this, an exhaustive analysis of the GaP crystals and the GaP/Si interfaces grown using different parameters (Table I) was carried out by means of TEM. The analyzed GaP crystals have been chosen with similar heights (around 100 nm) to be comparable.

Fig. 1 gathers the most representative images obtained for Sample 1 (Fig. 1a), and Sample 2 (Fig. 1b) by conventional Bright Field (BF) TEM analysis along the [110] zone axis.

Despite the different growth conditions and different substrate misorientations, the samples present a morphology analogous to island-like growth, showing both pyramidal and non-pyramidal features. Consequently, it could be stated that the morphology of the GaP crystals is not dominated by the range of temperatures studied in this batch of experiments, but by another mechanism. Moreover, there are no remarkable differences between samples in terms of density and type of defects. Specifically, planar defects, such as SFs and MTs were repeatedly observed along all the analyzed crystals. The origin of these defects could be due to some of the following factors: i) samples exhibit a 3D growth with a high amount of (111) GaP facets, so that when the islands grow they could be generating the MTs and SFs, ii) contamination (mainly O and C) at the GaP/Si interface due to their inefficient removal or iii) Si surface roughness due to pre-exposure with AsH_3.

To get a better understanding of the origin of these defects, and their relationship with the presence of contaminants on the Si surface before growth, high resolution TEM, high resolution STEM-HAADF and EELS measurements have been carried out on each sample along the [110] zone axis. Fig. 2 shows EELS false color maps of Si, O and C for the two samples in the areas where the defects were identified. The data suggest that some oxygen is present at the GaP/Si interface of Sample 1 (marked with a white arrow in Fig. 2a), whereas within measurement accuracy none was observed in similar regions on Sample 2. We note that except for adventitious surface contamination (derived, for example, from

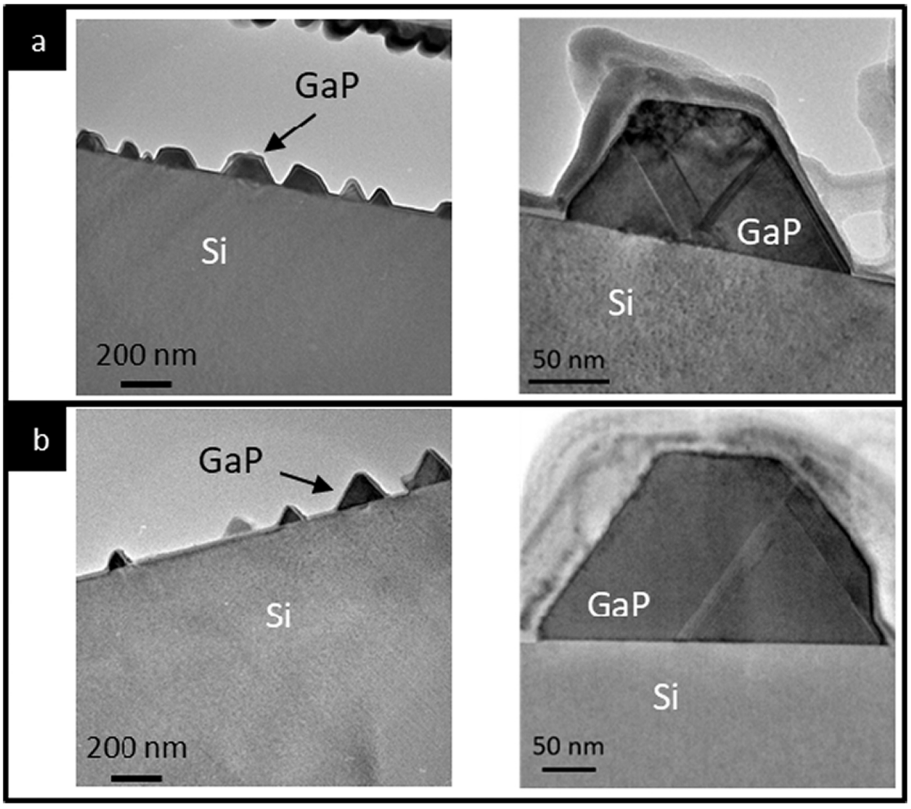

Fig. 1. Morphology of the GaP crystals in conventional BF TEM images along [110] zone axis of (a) Sample 1 (T = 700 °C, t = 2:30 min), and (b) Sample 2 (T = 725 °C and t = 2:30 min). Both samples present a similar morphology of the GaP crystals and the most common planar defects (stacking faults and microtwins) appear.

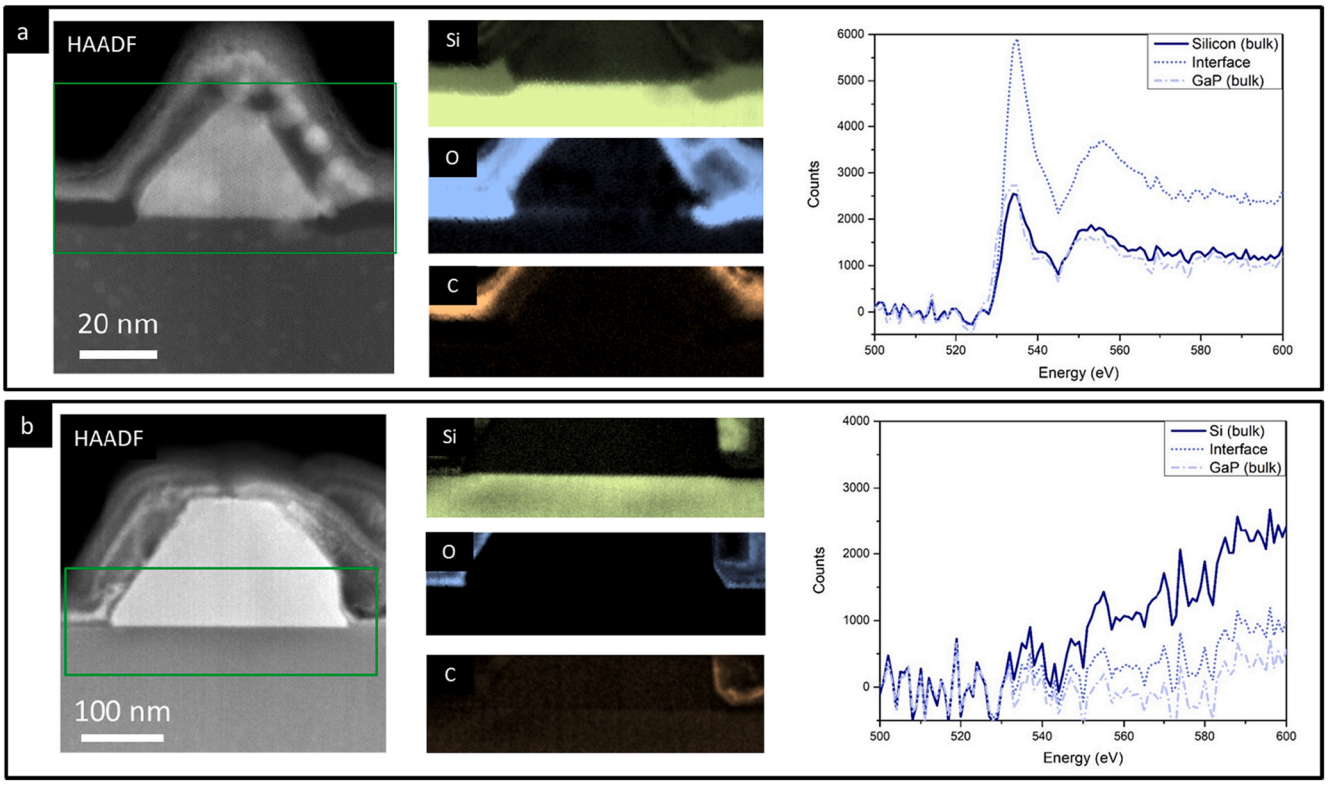

Fig. 2. HAADF images and EELS false color maps of one GaP crystal along [110] zone axis of a) Sample 1 ($T = 700$ °C, $t = 2{:}30$ min), and b) Sample 2 ($T = 725$ °C, t = 2:30 min). Oxygen is only detected in Sample 1 and carbon is not detected in any of the samples.

sample preparation), carbon was not detected in any of the samples.

To be more precise when determining the local presence of contaminants in the interface, EELS spectra have been evaluated in the three zones of interest for each sample. Fig. 3 shows the oxygen EELS spectra for Sample 1 (a) averaged over a representative area of 7.13 nm × 24.12 nm (171.98 nm^2) and Sample 2 (b) averaged over a representative area of 5.47 nm × 32.81 nm (179.47 nm^2), measured at three different points, namely: silicon substrate (thick line), GaP/Si interface (dotted line) and GaP layer (dashed line).

EELS spectra for Sample 1 revealed a significant peak of oxygen (532 eV) in the GaP/Si interface (dotted blue line), as it also observed in the false color map. The oxygen level does not drop to zero when moving out of the interface (i.e. on the Si substrate or on the GaP layer), meaning that the sample is slightly oxidized. Note that the content of oxygen, and thus the background level is similar on both cases (silicon substrate and GaP layer). Nonetheless, it is clearly visible that the oxygen peak in the GaP/Si interface is significantly larger than the background level, corroborating the presence of oxygen in the interface prior to growth.

On the other hand, EELS profiles measured on Sample 2 showed a null oxygen signal in the GaP/Si interface (dotted line). This observation agrees with the false color map, where no oxygen was detected on none of the three different areas. The fact that this element was not detected in our equipment can be explained either because there was not enough concentration to reach the detection threshold of the equipment or because the element was not present at all. In any case, the concentration is negligible as compared to Sample 1.

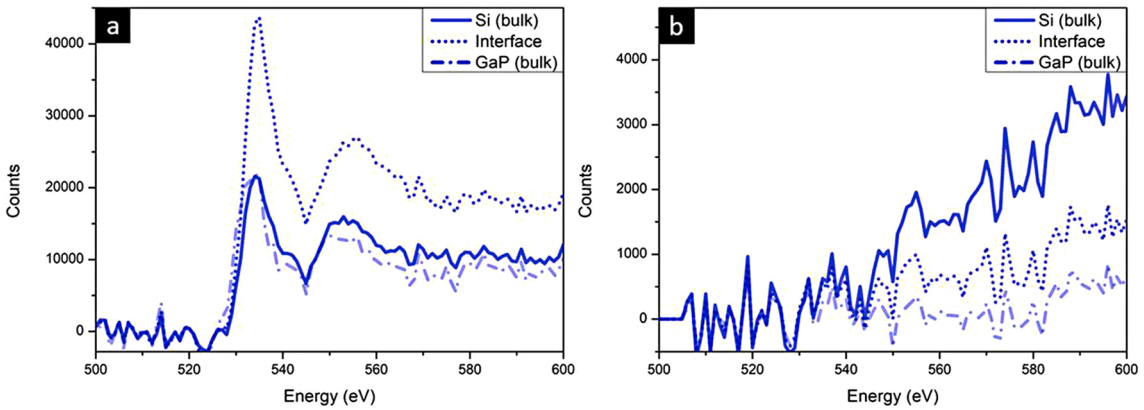

Fig. 3. Oxygen EELS spectra averaged over an area in the spectrum image in Fig. 2 measured in regions corresponding to the Si bulk, interface, and GaP layer for a) Sample 1 ($T = 700$ °C, $t = 2{:}30$ min), and b) Sample 2 ($T = 725$ °C, t = 2:30 min). There is remarkable oxygen at the GaP/Si interface of Sample 1, implying the presence of oxygen prior to the GaP growth. In contrast, there is no notable oxygen at the GaP/Si interface of Sample 2, so there is no oxygen contamination prior to the GaP growth.

These results (i.e., presence of oxygen in the interface of Sample 1, whose pre-exposure has the lowest temperature) supports the idea that the temperature plays a role on the deoxidation step [39],[44]. This agrees with previous results [27] in which the effectiveness of AsH_3 in removing oxygen from the surface at temperatures higher than 700 °C was observed by Auger Electron Spectroscopy.

Fig. 4 displays carbon EELS spectra for Sample 1 (a) and Sample 2 (b) averaged over the same representative area as Fig. 3 (a) and (b), respectively. In this case, the measurement of carbon levels at the three important points, namely: silicon substrate (thick line), GaP/Si interface (dotted line) and GaP layer (dashed line) have been compared to a carbon rich area. The presence of low levels of carbon contamination in both samples is suggested by a weak signal at the carbon ionization edge (K edge at 284 eV), regardless of the area where the analysis was performed (i.e., GaP layer, interface, and Si substrate) indicating a slight post-growth contamination of the sample (typically during preparation for TEM characterization), likely on the surface of the thinned specimen. Compared to the carbon edge strength observed in a region outside the GaP layer, corresponding to areas where traces of the bonding agents used for the cross-section preparation remain (clearly seen in the false color map of Fig. 2), it can be stated with confidence that the concentration of carbon present at the GaP/Si interface before the GaP growth was negligible on both samples.

In any case, it was observed that regardless of the presence (and quantity) of contaminants, the same type of defects (i.e., SFs and MTs) was detected in both samples. Consequently, it seems that the formation of planar defects, such as MTs, is not directly related to the existence of traces of O or C on the silicon surface, since these planar defects were formed in the two samples analyzed.

Having ruled out the existence of contaminants at the GaP/Si interface as a factor responsible for the formation of MTs, atomic chemical analysis was performed using atomically resolved EELS for the two samples to find out if the cause behind the origin of these defects lies in 3D growth. The measurements have been carried out in the area where the MT is formed and in the near surroundings, for comparison. Chemical maps were obtained from the Ga $L_{2,3}$ (edge onset at 1115 eV), P K (onset at 2143 eV) and Si K (onset at 1839 eV) edges. The relatively high energy loss onset of these edges ensures good signal localization, helping with the interpretation of the data in terms of atomically resolved relative concentration variations [45]. Note that the As $L_{2,3}$ edge (onset at 1323 eV) was in the energy range collected in the experiment, but no signal was detected, indicating the absence of As in the samples (within the instrumentation detection sensitivity).

Fig. 5 displays a representative STEM-HAADF image of Sample 2 along [110] zone axis. It can be seen that the MTs are clearly along the [111] direction and originate from the GaP/Si interface. It is important to remark that since all samples looked very similar, the data presented for Sample 2 is considered to be representative of all the samples examined (and the STEM-EELS data collected for Sample 1, not shown, is entirely consistent with the observations in Sample 2).

Two-dimensional chemical maps were obtained at one of the MT origins (solid square, Fig. 5b) and outside the planar defect at a position deemed visually 'clean' (i.e., a straight region of the interface devoid of defect: dashed square, Fig. 5c). For visual conciseness and to highlight the relative atomic column positions in the structure, RGB composites were created with the channels as follows: red (Ga $L_{2,3}$ edge at 1115 eV), green (P K edge at 2143 eV), blue (Si K edge at 1839 eV). Note that the map intensities are normalized, so that they reflect the relative localization of the Ga, P and Si columns but do not provide quantitative concentration information.

Fig. 5b (detailing the chemistry at the planar defect) shows extra Si intensity at the MT origin, coinciding with a drop in the Ga and P signals. This suggests that the MT origin has been reconstructed with extra Si present beyond the interface plane. Conversely, in straight interface regions (Fig. 5c), although the interface is quite sharp, there is systematically one or two layers of atomic columns where Si and Ga appear to be mixed. Considering that high energy ionization edges were used to generate these maps, which are less prone to delocalization, and the fact that the sample was thin (below 0.8 inelastic mean free path, as determined using the log-ratio method from low loss EELS data [46] acquired at the same position as the images and chemical maps, corresponding to ca. 35–40 nm thickness in all regions observed), it can be concluded that this is likely representative of some intermixing or mixed column occupancy at the interface across a couple of atomic planes. However, surface roughness in projection may additionally contribute to this observation and cannot be ruled out with certainty.

In addition to this chemical analysis, high-resolution HAADF-STEM images were recorded to reveal the atomic arrangements at the planar defects and their surroundings. Atomically high surface steps on the Si substrate, appearing as 'small darker bumps' similar to that observed at the position of the 2D EELS map in Fig. 5b at the origin of the MT, are observed all along the interface (Fig. 6), suggesting the substrate roughness may play a role in the formation of the observed defects. However, images in Fig. 6 from two different regions of Sample 2 illustrate the fact that the presence of these surface steps does not always lead to the formation of planar defects within the GaP, although it seems that the converse is true: the majority of MTs and planar defects observed terminate/originate at surface steps on the Si substrate. Therefore, 3D growth can be ruled out as the cause behind the origin of these defects.

To gain a deeper understanding of the atomic configuration of the GaP/Si interface, Fig. 7 presents high-resolution STEM images along the

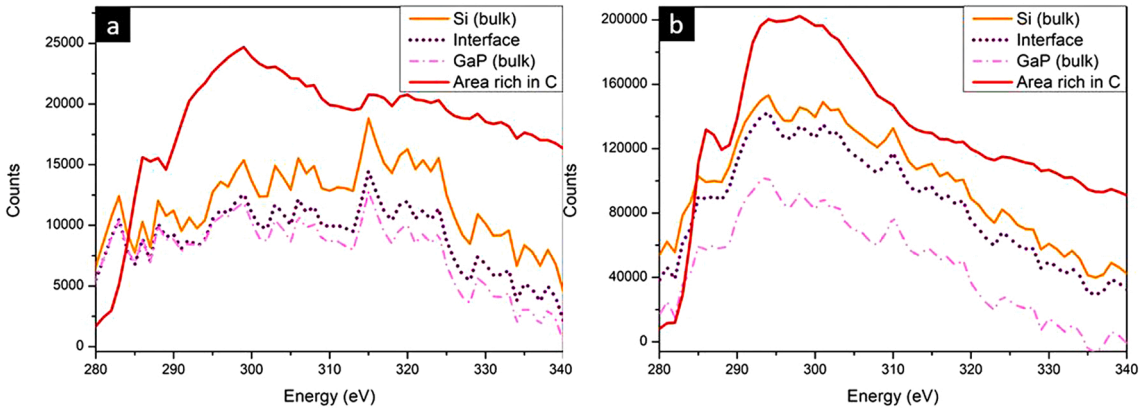

Fig. 4. Carbon EELS spectra averaged over an area in the spectrum image in Fig. 2 measured in regions corresponding to the Si bulk, interface, GaP layer and a region rich in carbon outside the GaP for a) Sample 1 (T = 700 °C, t = 2:30 min), and b) Sample 2 (T = 725 °C, t = 2:30 min). There is no remarkable carbon contamination at the GaP/Si interface in any of the samples, so there is no carbon contamination prior to the GaP growth.

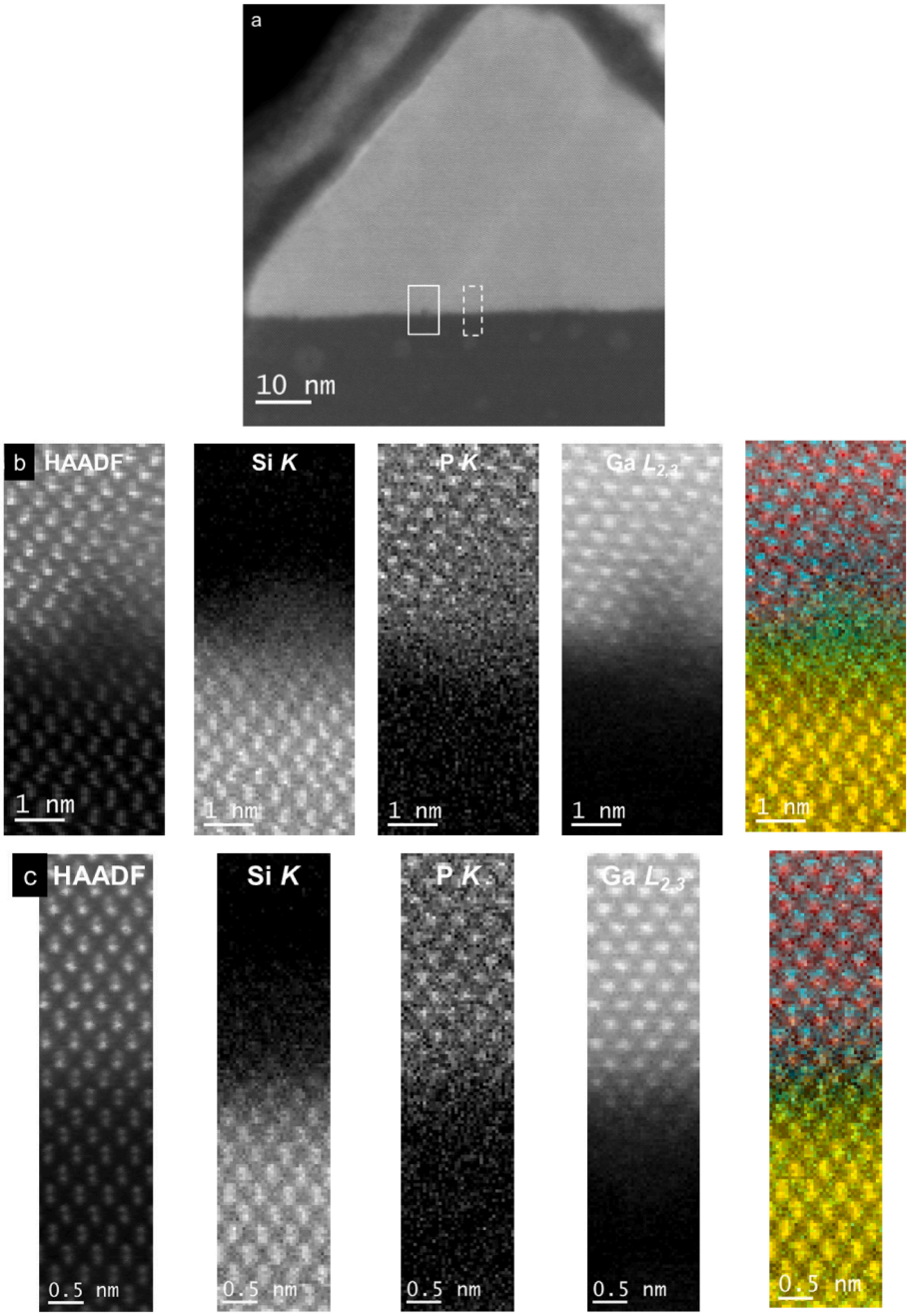

Fig. 5. EELS analysis of the origin of the MT observed on Sample 2 (T = 725 °C, t = 2:30 min) along the [110] zone axis. (a) HAADF overview image, showing the origin of the MT. The two areas where the compositional EELS 2D maps and simultaneously acquired HAADF intensity (b and c; the EELS intensity is normalized) were evaluated are highlighted by solid square (figure b, origin of the MT) and dashed square (figure c, outside the planar defect). The color composite combines the three individual maps with color channels as follows: red (Ga $L_{2,3}$ edge at 1115 eV), green (P K edge at 2143 eV), blue (Si K edge at 1839 eV), for convenient visualization. At the origin of the MT, extra Si is observed, which coincides with a drop in Ga and P. In contrast, outside the MT an intermixing of a couple of atomic columns of Si and Ga is observed. (For interpretation of the references to color in this figure legend, the reader is referred to the web version of this article.)

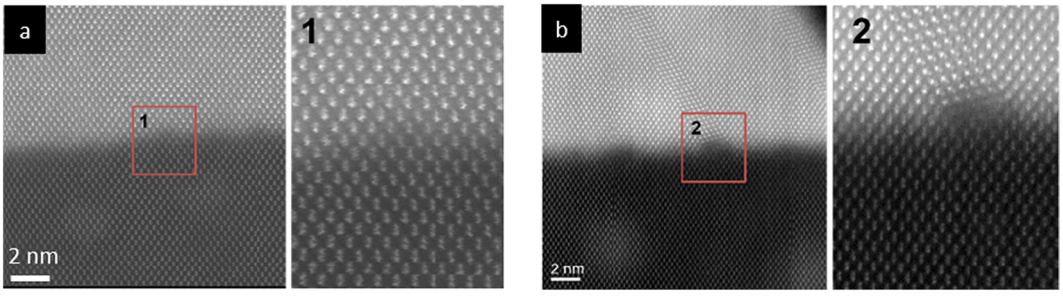

Fig. 6. High resolution STEM images of the [110] zone axis at the GaP/Si interface of Sample 2 (T = 725 °C, t = 2:30 min) of areas containing Si bumps where a) no planar defects were observed, b) a MT was present. Si bumps are areas where defects can or cannot be generated.

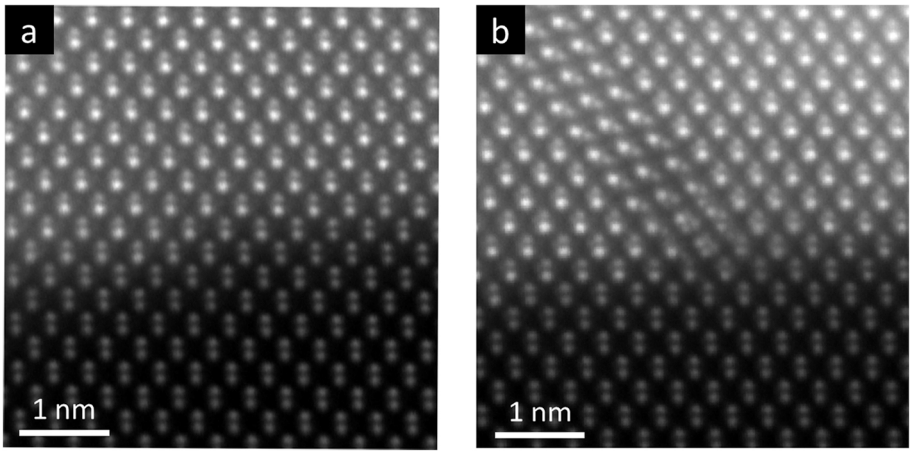

Fig. 7. High resolution HAADF STEM images at the GaP/Si interface of Sample 2 (T = 725 °C, t = 2:30 min) along the [110] zone axis. Fig. 7a corresponds to a defect-free region and Fig. 7b to an area where a MT has been detected. At the GaP/Si interface without defects there is an ordered transition between Si and GaP, while at the MT origin there is a complex atomic re-arrangement.

[110] zone axis of a defect-free region (a) and of a region where a defect is emerging (b). As can be clearly observed from the HAADF image contrast (which scales with the atomic number Z of the observed elements as Z^n, n = 1.5–2 [47],[48]), in the defect-free region and the surroundings of the defect there is no change in polarity of the dumbbells, i.e., there is no inversion of the Ga—P polarity, and therefore no anti-phase domains (APDs) are observed. Fig. 7a reveals a sharp and ordered transition between Si and GaP, along the interface, including Si atomic step. In contrast, Fig. 7b shows a complex atomic rearrangement at the interface where the defect originates.

Using the Z dependence of the HAADF intensity as a qualitative guide to provide a chemical assignment at each atomic column, and considering that Z_{As} = 33, Z_{Ga} = 31, ZP = 15, and Z_{Si} = 14, we can build an idealized (and likely simplified) atomic model of the interface structures gathered in Fig. 7. This assignment is shown in Fig. 8 for a zone outside the defect (Fig. 8b) and another at the beginning of the defect (Fig. 8e). Fig. 8b and d show HAADF profiles along the lines marked in Fig. 8a, namely a dashed line outside the defect and a solid green line along the defect, respectively. Fig. 8c and e correspond to a detail of the interface (extracted from Fig. 8a) with superimposed colored circles indicating a proposed assignment of the three-existing types of atomic columns (silicon: yellow circles; gallium: red circles; and phosphorous: blue circles), outside the defect and in the defect, respectively, which will be discussed below.

According to [49], there are two different configurations (polarities) for the arrangement of Ga and P atoms in a GaP layer grown on Si (i.e. Case A➔B and Case B➔A) as described in Fig. 9. According to the distribution of the Ga—P 'dumbbells' in our samples, they can be certainly classified as Case B➔ A (Fig. 9).

On the other hand, depending on the nature of the atoms at the

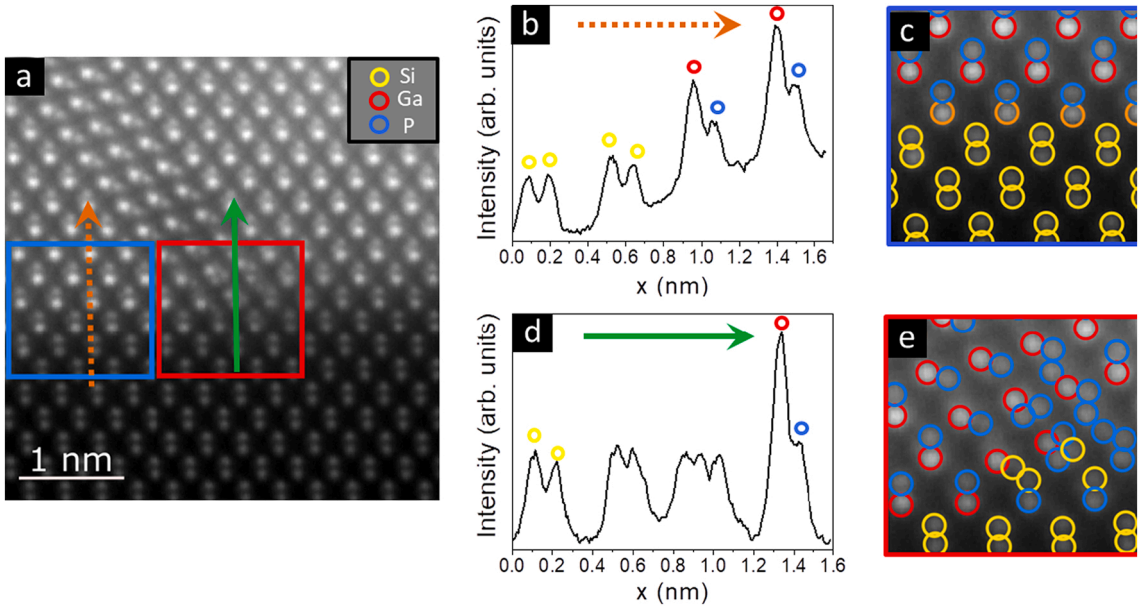

Fig. 8. High resolution investigation of the onset of a MT at the GaP/Si interface of Sample 2 (T = 725 °C, t = 2:30 min) along the [110] zone axis. (a) HAADF image highlighting the areas (blue outside the MT and red at the origin of the MT) where the atoms (Ga, P and Si) have been identified and the lines where the intensity profiles have been taken. (b) and (d) intensity profiles analysis outside the MT and at the origin of the MT, respectively. (c) and (e) detail of the interface highlighting the three-existing type of atoms, outside the MT and at the MT origin, respectively. Yellow circles are for Si, red circles for Ga and blue circles for P. It is observed an intermixing of Ga and Si outside the MT and a complex atomic structure composed of groups of three or four atoms at the beginning of the MT. (For interpretation of the references to color in this figure legend, the reader is referred to the web version of this article.)

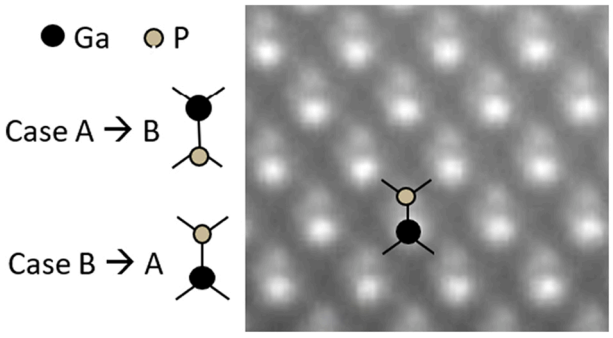

Fig. 9. Configurations reported in [2] for the arrangement of Ga and P atoms in a GaP layer grown on silicon substrates by MOVPE. On the right, high resolution STEM image of Sample 2, evidencing that Ga—P dumbbells are organized following Case B➔A.

silicon surface, there are two proposed structures [49], named 'abrupt' or 'compensated', depending on whether the Si bonds to P (abrupt) or both Ga/P alternatively (compensated), the latter being the most stable configuration (Fig. 10). Fig. 8c, clearly demonstrates that in the defect-free region, that the GaP starts with Ga, since the Ga- (or Ga-rich) columns can be easily identified due to their brighter intensity, as Z_{Ga} is much higher in comparison with P or Si (Fig. 8). However, a slightly lower intensity is observed in the first atomic plane in direct contact with the Si, compared to the Ga columns in the 'bulk' GaP region. This could be explained with the "compensated" configuration, in which Ga atoms are intercalated with Si, resulting in an attenuation of *Z*-contrast compared to that of a column consisting of just Ga atoms. Additionally, the EELS results highlighted some level of chemical mixing within a couple of atomic layers at the interface. All this suggests that the GaP/Si interface observed can be classified as Case B➔A compensated.

Based on the data and the analysis presented, it can be suggested that the nucleation of the GaP layer starts with a Ga—Si bond, which is a surprising fact given that the growth procedure started in all the samples with exposure to PH_3. This can be explained by surface exposure to AsH_3, which favors Ga—Si bonds at the expense of P—Si bonds. On the other hand, the Ga—Si bonds arrangement is interrupted in the defect region (Fig. 8a).

A high magnification detail of the onset of the MT in Fig. 8e suggests the presence of groups of three and four atomic columns just at the beginning of the defect. The exact chemical nature of the atomic columns in this reconstructed region is difficult to establish with certainty. Several combinations of elements can lead to a similar Z contrast in projection, and unlike the pure GaP and Si regions, the onsets of defects are sensitive to the electron beam, making atomically resolved EELS analysis difficult in the conditions we used. Purely based on a qualitative comparison of HAADF intensities, and assuming pure columns (as opposed to mixed occupancy), we proposed a tentative assignment on Fig. 8e. This simplistic model illustrates the fact that the roughness of the Si substrate surface can favor P bonding to the silicon surface by revealing higher index planes. This also considers our EELS analysis which reveal the presence of Si inside the GaP layer, within the region of the planar defect. This in turn could be related to Si diffusion from the substrate to the epitaxial layer through defects, as previously reported by [50].

A search for structures using ab initio methods, combined with image simulations of the candidate structures, may provide further clues and a more definitive assignment of the chemistry of these atomic columns, but such a study is beyond the context of this work.

Finally, it is important to comment that no traces of As were detected in any of the EELS measurements. This observation is consistent with the hypothesis that As dimers are completely displaced when TMGa or/and PH_3 are introduced in the MOVPE reactor at the beginning of GaP growth [27],[37],[51] or that the As desorbs out of the Si surface due to the high temperature used [52]. In fact, it is most likely that Ga atoms are the responsible for As atoms displacement since the growth starts with Ga—Si bonds.

In view of all these results, it could be concluded that:

i. AsH_3 pre-exposure and a growth temperature of 725 °C are sufficient to achieve a surface free of contaminants (O and C).
ii. The use of As-pre-exposure does not create intermediate GaAsP compounds. Moreover, no As is detected in the GaP/Si interface. This is most likely due to the fact that when TMGa is let into the reactor chamber, Ga atoms effectively displace As, which is totally removed from the growth surface. This is consistent with the fact that the GaP on Si growth starts with Ga—Si bonds for all AsH_3 flows and growth temperatures under study.
iii. The formation of stacking faults on GaP on Si appears linked to the interruption of Ga—Si bonds in the Si surface, an effect that might be enhanced on Si rough surfaces.

These results increase the knowledge and understanding of the phenomena behind the formation of GaP defects on Si grown by MOVPE, with a view to designing an optimal procedure transferable to the photovoltaic industry.

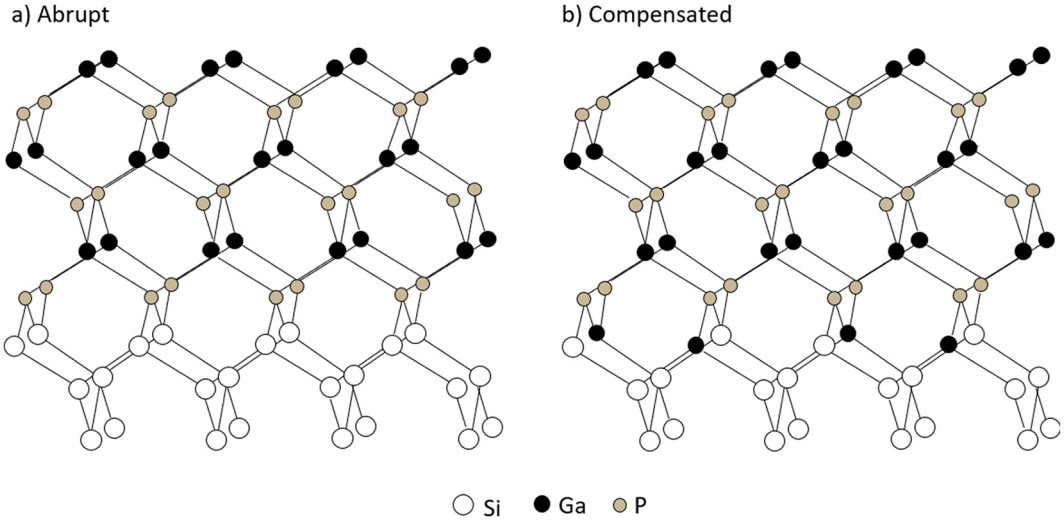

Fig. 10. Diagrams of the possible interface models reported in [1] for case B➔ A GaP layer grown on silicon substrate by MOVPE.

4. Summary and conclusions

The use of AsH_3 pre-exposure in high-temperature epitaxial growth of GaP layers on silicon substrates shows very promising properties for the integration of III-V compounds on silicon to develop high efficiency and cost-effective tandem solar cells. However, epitaxial processes using AsH_3 pre-exposure as cleaning and substrate conditioning steps suffer from reproducibility and robustness issues. The effect of different AsH_3 pre-exposure parameters (i.e. temperature and time) on the morphological and structural quality of the GaP layer have been studied. All samples studied in this paper presented an island-like growth, combining the presence of pyramidal and non-pyramidal shapes. In all cases it has been observed that the only types of planar defects appearing in the GaP crystals were SFs and MTs. No APDs have been found throughout all the GaP crystals analyzed.

Despite the similarities between the samples regarding the formation of planar defects, it has been observed that when the samples are exposed to temperatures lower than 725 °C, some contaminants (mainly O) remain on the Si surface. On the other hand, samples subjected to higher temperatures (i.e. $>$ 725 °C) did not show these contaminants, confirming that pre-exposure to AsH_3 helps in the Si deoxidation. This fact leads to the conclusion that the formation of planar defects is not related to the presence of O in the GaP/Si interface, as this type of defects was observed in all cases, regardless the presence of O.

Finally, planar defects have been analyzed by high-resolution STEM and EELS to achieve a better understanding of their origin and nature. The combination of the different techniques reveals that GaP crystals start with Ga at the GaP/Si interface, following a so-called "compensated" atomic bonding model. On the contrary, a complex atomic distribution is observed at the GaP/Si interface where the planar defects originate. This set of results confirms that for these growth conditions, GaP nucleation begins with the Ga—Si bond and, consequently, the formation of planar defects could be linked to the interruption of Ga dimers on the Si surface, an effect which could be triggered by the roughness of the Si surface.

CRediT authorship contribution statement

Amalia Navarro: Investigation, Writing – original draft, Writing – review & editing, Visualization, Formal analysis, Conceptualization. **Elisa García-Tabarés:** Writing – original draft, Writing – review & editing, Visualization, Conceptualization. **Quentin M. Ramasse:** Resources, Formal analysis, Methodology, Software, Writing – review & editing, Data curation. **Pablo Caño:** Resources, Writing – review & editing. **Ignacio Rey-Stolle:** Resources, Writing – review & editing, Funding acquisition, Conceptualization. **Beatriz Galiana:** Supervision, Project administration, Writing – review & editing, Funding acquisition, Conceptualization, Data curation.

Declaration of Competing Interest

The authors declare that they have no known competing financial interests or personal relationships that could have appeared to influence the work reported in this paper.

Data availability

No data was used for the research described in the article.

Acknowledgements

This work was supported by the Spanish Ministerio de Ciencia e Innovación through project DAMAINSOL [grant number RTI2018-101020-B-I00], the Regional Government of Madrid through TECHNOFUSIÓN(*III*)CM (S2018/EMT-4437) and Comunidad de Madrid (Spain) multiannual agreement with UC3M, "Excelencia para el Profesorado Universitario" (EPUC3M14) - Fifth regional research plan 2016-2020. IR-S acknowledges the support provided by the Spanish Ministerio de Ciencia e Innovación through project VIGNEMALE [grant number RTI2018-094291-B-I00]. STEM-EELS was carried out at SuperSTEM, the UK National Facility for Advanced Electron Microscopy, supported by EPSRC.

STEM-EELS was carried out at SuperSTEM, the UK National Facility for Advanced Electron Microscopy, supported by EPSRC.

References

[1] J.E. Ayers, T. Kujofsa, P. Rago, J. Raphael, Heteroepitaxy of Semiconductors, 2016, https://doi.org/10.1201/9781315372440.
[2] Y.B. Bolkhovityanov, O.P. Pchelyakov, GaAs epitaxy on Si substrates: modern status of research and engineering, Physics-Uspekhi. 51 (2008) 437–456, https://doi.org/10.1070/pu2008v051n05abeh006529.
[3] T. Soga, T. Jlmbo, M. Umeno, Epitaxial growth of a two-dimensional structure of GaP on Si substrate by metalorganic chemical vapor deposition, Appl. Surf. Sci. 82 (83) (1994) 64–69, https://doi.org/10.1143/JJAP.33.6654.
[4] J.-W. Lee, J. Salzman, D. Emerson, J.R. Shealy, J.M. Ballantyne, Selective Area Growth of GaP on Si by MOCVD, 1997.
[5] T. Suzuki, T. Soga, T. Jimbo, M. Umeno, Growth mechanism of GaP on Si substrate by MOVPE, J. Cryst. Growth 115 (1991) 158–163, https://doi.org/10.1016/0022-0248(91)90731-J.
[6] H. Kroemer, POLAR-ON-NONPOLAR EPITAXY, J. Cryst. Growth 81 (1987) 193–204.
[7] M. Feifel, D. Lackner, J. Schön, J. Ohlmann, J. Benick, G. Siefer, F. Predan, M. Hermle, F. Dimroth, Epitaxial GaInP/GaAs/Si triple-junction solar cell with 25.9% AM1.5g efficiency enabled by transparent metamorphic AlxGa1−xAsyP1−y step-graded buffer structures, Sol. RRL 5 (2021) 1–7, https://doi.org/10.1002/solr.202000763.
[8] D.L. Lepkowski, T.J. Grassman, J.T. Boyer, D.J. Chmielewski, C. Yi, M.K. Juhl, A. H. Soeriyadi, N. Western, H. Mehrvarz, U. Römer, A. Ho-Baillie, C. Kerestes, D. Derkacs, S.G. Whipple, A.P. Stavrides, S.P. Bremner, S.A. Ringel, 23.4% monolithic epitaxial GaAsP/Si tandem solar cells and quantification of losses from threading dislocations, Sol. Energy Mater. Sol. Cells 230 (2021) 1–9, https://doi.org/10.1016/j.solmat.2021.111299.
[9] S. Fan, Z.J. Yu, Y. Sun, W. Weigand, P. Dhingra, M. Kim, R.D. Hool, E.D. Ratta, Z. C. Holman, M.L. Lee, 20%-efficient epitaxial GaAsP/Si tandem solar cells, Sol. Energy Mater. Sol. Cells 202 (2019), 110144, https://doi.org/10.1016/j.solmat.2019.110144.
[10] R. Jones, P. Doussiere, J.B. Driscoll, W. Lin, H. Yu, Y. Akulova, T. Komljenovic, J. E. Bowers, Heterogeneously integrated InP/silicon photonics: fabricating fully functional transceivers, IEEE Nanotechnol. Mag. 13 (2019) 17–26, https://doi.org/10.1109/MNANO.2019.2891369.
[11] R. Cariou, J. Benick, P. Beutel, N. Razek, C. Flotgen, M. Hermle, D. Lackner, S. W. Glunz, A.W. Bett, M. Wimplinger, F. Dimroth, Monolithic two-terminal III-V//Si triple-junction solar cells with 30.2% efficiency under 1-Sun AM1.5g, IEEE J. Photovolt. 7 (2017) 367–373, https://doi.org/10.1109/JPHOTOV.2016.2629840.
[12] S. Essig, C. Allebé, T. Remo, J.F. Geisz, M.A. Steiner, K. Horowitz, L. Barraud, J. S. Ward, M. Schnabel, A. Descoeudres, D.L. Young, M. Woodhouse, M. Despeisse, C. Ballif, A. Tamboli, Raising the one-sun conversion efficiency of III-V/Si solar cells to 32.8% for two junctions and 35.9% for three junctions, Nat. Energy 2 (2017), https://doi.org/10.1038/nenergy.2017.144.
[13] M. Green, E. Dunlop, J. Hohl-Ebinger, M. Yoshita, N. Kopidakis, X. Hao, Solar cell efficiency tables (version 57), Prog. Photovolt. Res. Appl. 29 (2021) 3–15, https://doi.org/10.1002/pip.3371.
[14] B. Shi, L. Wang, A.A. Taylor, S. Suran Brunelli, H. Zhao, B. Song, J. Klamkin, MOCVD grown low dislocation density GaAs-on-V-groove patterned (001) Si for 1.3 μ m quantum dot laser applications, Appl. Phys. Lett. 114 (2019) 3–8, https://doi.org/10.1063/1.5090437.
[15] M. Vaisman, N. Jain, Q. Li, K.M. Lau, E. Makoutz, T. Saenz, W.E. Mcmahon, A. C. Tamboli, E.L. Warren, GaAs solar cells on nanopatterned Si substrates, IEEE J. Photovolt. 8 (2018) 1635–1640, https://doi.org/10.1109/JPHOTOV.2018.2871423.
[16] S.A. Ringel, J.A. Carlin, C.L. Andre, M.K. Hudait, M. Gonzalez, D.M. Wilt, E. B. Clark, P. Jenkins, D. Scheiman, A. Allerman, E.A. Fitzgerald, C.W. Leitz, Single-junction InGaP/GaAs solar cells grown on Si substrates with SiGe buffer layers, Prog. Photovolt. Res. Appl. 10 (2002) 417–426, https://doi.org/10.1002/pip.448.
[17] M. Yamaguchi, K.H. Lee, K. Araki, N. Kojima, A review of recent progress in heterogeneous silicon tandem solar cells, J. Phys. D. Appl. Phys. 51 (2018), 133002, https://doi.org/10.1088/1361-6463/aaaf08.
[18] T.J. Grassman, J.A. Carlin, B. Galiana, L. Yang, F. Yang, M.J. Mills, S.A. Ringel, Nucleation-related defect-free GaP / Si (100) heteroepitaxy via metal-organic chemical vapor deposition, Appl. Phys. Lett. 102 (2013) 1–4.
[19] T. Soga, T. Jimbo, M. Umeno, Dislocation generation mechanisms for GaP on Si grown by metalorganic chemical vapor deposition, Appl. Phys. Lett. 63 (1993) 2543–2545, https://doi.org/10.1063/1.110427.
[20] A. Beyer, I. Németh, S. Liebich, J. Ohlmann, W. Stolz, K. Volz, Influence of crystal polarity on crystal defects in GaP grown on exact Si (001), J. Appl. Phys. 109 (2011) 1–7, https://doi.org/10.1063/1.3567910.

[21] Y. Kohama, Y. Kadota, Y. Ohmachi, Initial stages of epitaxial growth of GaP on Si with AsH3 Preflow, Jpn. J. Appl. Phys. 29 (1990) L229–L232, https://doi.org/10.1143/JJAP.29.L229.
[22] I. Németh, B. Kunert, W. Stolz, K. Volz, Heteroepitaxy of GaP on Si: correlation of morphology, anti-phase-domain structure and MOVPE growth conditions, J. Cryst. Growth 310 (2008) 1595–1601, https://doi.org/10.1016/j.jcrysgro.2007.11.127.
[23] H. Döscher, S. Brückner, T. Hannappel, Investigation of oxide removal from Si (100) substrates in dependence of the MOVPE process gas ambient, J. Cryst. Growth 318 (2011) 563–569, https://doi.org/10.1016/j.jcrysgro.2010.11.087.
[24] K. Volz, A. Beyer, W. Witte, J. Ohlmann, I. Németh, B. Kunert, W. Stolz, GaP-nucleation on exact Si (001) substrates for III / V device integration, J. Cryst. Growth 315 (2011) 37–47, https://doi.org/10.1016/j.jcrysgro.2010.10.036.
[25] O. Supplie, O. Romanyuk, C. Koppka, M. Steidl, A. Nägelein, A. Paszuk, L. Winterfeld, A. Dobrich, P. Kleinschmidt, E. Runge, T. Hannappel, Metalorganic vapor phase epitaxy of III–V-on-silicon: experiment and theory, Prog. Cryst. Growth Charact. Mater. 64 (2018) 103–132, https://doi.org/10.1016/j.pcrysgrow.2018.07.002.
[26] T.E. Saenz, W.E. McMahon, A.G. Norman, C.L. Perkins, J.D. Zimmerman, E. L. Warren, High-temperature nucleation of GaP on V-grooved Si, Cryst. Growth Des. 20 (2020) 6745–6751, https://doi.org/10.1021/acs.cgd.0c00875.
[27] E.L. Warren, A.E. Kibbler, R.M. France, A.G. Norman, P. Stradins, W.E. McMahon, Growth of antiphase-domain-free GaP on Si substrates by metalorganic chemical vapor deposition using an in situ AsH3 surface preparation, Appl. Phys. Lett. 107 (2015), 082109, https://doi.org/10.1063/1.4929714.
[28] A. Navarro, E. García-Tabarés, B. Galiana, P. Caño, I. Rey-Stolle, C. Ballesteros, MOVPE growth of GaP on Si with as initial coverage, J. Cryst. Growth 464 (2017) 8–13, https://doi.org/10.1016/j.jcrysgro.2016.11.077.
[29] Y.T. Sun, S. Lourdudoss, Epitaxial Lateral Overgrowth of III-V Semiconductors on Si for Photonic Integration, 1st ed, Elsevier Inc., 2019, https://doi.org/10.1016/bs.semsem.2019.07.004.
[30] H. Döscher, P. Kleinschmidt, T. Hannappel, Atomic surface structure of Si(1 0 0) substrates prepared in a chemical vapor environment, Appl. Surf. Sci. 257 (2010) 574–580, https://doi.org/10.1016/j.apsusc.2010.07.035.
[31] B. Kunert, I. Németh, S. Reinhard, K. Volz, W. Stolz, Si (001) surface preparation for the antiphase domain free heteroepitaxial growth of GaP on Si substrate, Thin Solid Films 517 (2008) 140–143, https://doi.org/10.1016/j.tsf.2008.08.077.
[32] M. Deura, Y. Kondo, M. Takenaka, S. Takagi, Y. Shimogaki, Y. Nakano, M. Sugiyama, High-temperature annealing effect of Si in group-V ambient prior to heteroepitaxy of InAs in metal-organic vapor phase epitaxy, Jpn. J. Appl. Phys. 50 (2011), https://doi.org/10.1143/JJAP.50.04DH07.
[33] E. García-Tabarés, I. García, D. Martín, I. Rey-Stolle, Influence of PH3 exposure on silicon substrate morphology in the MOVPE growth of III-V on silicon multijunction solar cells, J. Phys. D. Appl. Phys. 46 (2013), https://doi.org/10.1088/0022-3727/46/44/445104.
[34] Y. Takano, K. Morizumi, S. Watanabe, H. Masuda, T. Okamoto, K. Noda, S. Fukuda, T. Ozeki, K. Kuwahara, S. Fuke, Y. Furukawa, H. Yonezu, High-temperature growth of GaP on Si substrates by metalorganic vapor phase epitaxy, Jpn. J. Appl. Phys. 48 (2009), https://doi.org/10.1143/JJAP.48.011102.
[35] K. Yamane, T. Kobayashi, Y. Furukawa, H. Okada, H. Yonezu, A. Wakahara, Growth of pit-free GaP on Si by suppression of a surface reaction at an initial growth stage, J. Cryst. Growth 311 (2009) 794–797, https://doi.org/10.1016/j.jcrysgro.2008.09.097.
[36] W.E. McMahon, E.L. Warren, A.E. Kibbler, R.M. France, A.G. Norman, R.C. Reedy, J.M. Olson, A.C. Tamboli, P. Stradins, Surfaces and interfaces governing the OMVPE growth of APD-free GaP on AsH3-cleaned vicinal Si(100), J. Cryst. Growth 452 (2016) 235–239, https://doi.org/10.1016/j.jcrysgro.2016.05.014.
[37] P. Caño, C.M. Ruiz, A. Navarro, B. Galiana, I. García, I. Rey-stolle, Growth of GaP layers on Si substrates in a standard MOVPE reactor for multijunction solar cells, Coatings. 11 (2021) 1–13.
[38] A. Paszuk, P. Kleinschmidt, T. Hannappel, T. Hannappel, O. Supplie, S. Bruckner, M.M. May, A. Dobrich, A. Nagelein, B. Kim, Y. Nakano, M. Sugiyama, In Situ Control over the Sublattice Orientation of GaP/Si(100): As Virtual Substrates for Tandem Absorbers, 2018, pp. 2538–2542, https://doi.org/10.1109/pvsc.2017.8366561.
[39] T. Hannappel, W.E. McMahon, J.M. Olson, An RDS, LEED, and STM study of MOCVD-prepared Si(1 0 0) surfaces, J. Cryst. Growth 272 (2004) 24–29, https://doi.org/10.1016/j.jcrysgro.2004.08.043.
[40] A. Beyer, K. Volz, Advanced Electron microscopy for III/V on silicon integration, Adv. Mater. Interfaces 6 (2019), https://doi.org/10.1002/admi.201801951.
[41] M. Feifel, J. Ohlmann, R.M. France, D. Lackner, F. Dimroth, Electron channeling contrast imaging investigation of stacking fault pyramids in GaP on Si nucleation layers, J. Cryst. Growth 532 (2020), https://doi.org/10.1016/j.jcrysgro.2019.125422.
[42] J.T. Boyer, A.N. Blumer, Z.H. Blumer, D.L. Lepkowski, T.J. Grassman, Correlation of early-stage growth process conditions with dislocation evolution in MOCVD-based GaP/Si heteroepitaxy, J. Cryst. Growth 571 (2021), 126251, https://doi.org/10.1016/j.jcrysgro.2021.126251.
[43] M.S.A. Paszuk, Controlling Si(111) and Si(100) Surfaces for Subsequent GaP Heteroepitaxy in CVD Ambient, 2017.
[44] A. Paszuk, O. Supplie, B. Kim, S. Brückner, M. Nandy, A. Heinisch, P. Kleinschmidt, Y. Nakano, M. Sugiyama, T. Hannappel, GaAsP/Si tandem solar cells: In situ study on GaP/Si:As virtual substrate preparation, Sol. Energy Mater. Sol. Cells 180 (2018) 343–349, https://doi.org/10.1016/j.solmat.2017.07.032.
[45] P. Wang, A.J. D'Alfonso, S.D. Findlay, L.J. Allen, A.L. Bleloch, Contrast reversal in atomic-resolution chemical mapping, Phys. Rev. Lett. 101 (2008) 1–4, https://doi.org/10.1103/PhysRevLett.101.236102.
[46] R.F. Egerton, Electron energy-loss spectroscopy in the electron microscope, Electron. Energy Loss Spectrosc. Electron Microsc. (2011), https://doi.org/10.1007/978-1-4419-9583-4.
[47] E.J. Kirkland, Advanced Computing in electron Microscopy, Second edition, Springer US, 2010, https://doi.org/10.1007/978-1-4419-6533-2.
[48] P. Hartel, H. Rose, C. Dinges, Conditions and reasons for incoherent imaging in STEM, Ultramicroscopy. 63 (1996) 93–114, https://doi.org/10.1016/0304-3991(96)00020-4.
[49] O. Supplie, S. Brückner, O. Romanyuk, H. Döscher, C. Höhn, M.M. May, P. Kleinschmidt, F. Grosse, T. Hannappel, Atomic scale analysis of the GaP/Si(100) heterointerface by in situ reflection anisotropy spectroscopy and ab initio density functional theory, Phys. Rev. B Condens. Matter Mater. Phys. 90 (2014) 1–8, https://doi.org/10.1103/PhysRevB.90.235301.
[50] Y. Kohama, K. Uchida, T. Soga, T. Jimbo, M. Umeno, Quality improvement of metalorganic chemical vapor deposition grown GaP on Si by AsH3 preflow 53, 1988, pp. 10–13, https://doi.org/10.1063/1.100096.
[51] E.L. Warren, E.A. Makoutz, T. Saenz, M. Martirossyan, A. Neumann, K. Horowitz, A. Matheson, A. Norman, A.C. Tamboli, J.D. Zimmerman, W.E. McMahon, Enabling low-cost III-V/Si integration through nucleation of GaP on v-grooved Si substrates, in: 2018 IEEE 7th World Conf. Photovolt. Energy Conversion, WCPEC 2018 - A Jt. Conf. 45th IEEE PVSC, 28th PVSEC 34th EU PVSEC, 2018, pp. 268–270, https://doi.org/10.1109/PVSC.2018.8547324.
[52] O. Supplie, M.M. May, P. Kleinschmidt, A. Nägelein, A. Paszuk, S. Brückner, T. Hannappel, In situ controlled heteroepitaxy of single-domain GaP on As-modified Si(100), APL Mater. 3 (2015), https://doi.org/10.1063/1.4939005.